COBEM 2023 27TH INTERNATIONAL CONGRESS OF MECHANICAL ENGENEERING

ABCM Brazilian Society of Mechanical Sciences and Engineering
27th ABCM International Congress of Mechanical Engineering
December 04-08, 2023, Florianópolis-SC, Brazil

COB-2023-2010 Numerical and Experimental Assessment of a Hybrid Active Magnetic Regenerator Assembled with Gd and La-Fe-Si alloys

Rogerio S. Sucaria
Paulo V. de Faria
Bernardo P. Vieira
Higor F. Teza
Jaime A. Lozano
Jader R. Barbosa Jr.

POLO – Research Laboratories for Emerging Technologies in Cooling and Thermophysics, Department of Mechanical Engineering, Federal University of Santa Catarina, Florianópolis – SC, Brazil

rogerio.sucaria@polo.ufsc.br, paulo.faria@polo.ufsc.br, bernardo.vieira@polo.ufsc.br, jaime@polo.ufsc.br, jrb@polo.ufsc.br

Abstract. *Active magnetic regenerators are the central part of magnetocaloric refrigerators, being responsible for housing the solid refrigerant and generating cooling capacity through cyclic changes in flow direction and applied magnetic field. Gadolinium is one of the most consolidated refrigerants, but La-Fe-Si alloys have gained prominence in recent years. In this study, an active regenerator numerical model was adapted to simulate multi-material (hybrid) regenerators through adjustments in its mesh generation. A real hybrid regenerator was then assembled with one layer of Gd and ten layers of La-Fe-Si alloys with different Curie temperatures. It was then experimentally tested in an existing regenerator testing apparatus and the results were compared with the ones obtained by the model, aiming to validate it. The model showed good agreement with the experimental data in regards to the behavior of the cooling capacity and the maximum temperature span, but showed limitations with precisely predicting the cooling capacity values. The difference in cooling capacity, however, did not exceed 8.2 W and was fairly low in most cases. The results also indicated that hybrid regenerators might be able to reach higher temperature spans than their single-material counterparts.*

Keywords: *Magnetic Refrigeration, Hybrid Active Magnetic Regenerator, Numerical Modeling.*

1. INTRODUCTION

Magnetic refrigeration systems are an alternative cooling technology based on the Magnetocaloric Effect (MCE) that have seen a rise in prominence for room temperature applications in the last decades. This rise is seen as a response to some of the several limitations presented by conventional refrigeration systems, which utilize mechanical compression of volatile fluids, such as low-efficiency and the use of potentially harmful refrigerants that may be flammable, toxic or dangerous for the environment. Magnetic refrigeration systems solve or mitigate these problems through their potential for high efficiency due to the reversible nature of the magnetocaloric effect, and the use of recyclable, solid refrigerants, which are more environmentally friendly and do not present the risk of leakage (Smith *et al.*, 2012).

The magnetocaloric effect is characterized as a thermal response that all magnetic materials present when submitted to a change in magnetic field, usually translated into a temperature change (if the process is isentropic) or heat absorption/rejection (if the process is isothermal) (Smith *et al.*, 2012). One of the ways to utilize this effect in refrigeration applications is through the use of Active Magnetic Regenerators (AMRs), which consist of a porous medium comprised of a solid refrigerant, known as the Magnetocaloric Material (MCM). The most common MCMs are Gadolinium (Gd) and Lanthanum-Iron-Silicon (La-Fe-Si) alloys, mainly due to their fairly good magnetocaloric properties, which include a Curie temperature (the temperature in which the MCE is maximum) near room temperature, and that may be tuned through changes in the composition of the materials (Bjørk *et al.*, 2010; Hansen *et al.*, 2010; Kitanovski *et al.*, 2015; Vieira *et al.*, 2021).

The AMR is one of the main components of most magnetic refrigeration systems and operates under the AMR cycle, a Brayton thermo-magnetic cycle comprised of two adiabatic and two iso-field processes, with the MCM acting as both refrigerant and heat storage (Kitanovski *et al.*, 2015; Vieira *et al.*, 2023). The first step of the cycle is the adiabatic magnetization, in which a magnetic field is applied to the AMR and the material within it increases its temperature through the MCE. This is followed by the cold blow, in which fluid from the cold reservoir flows through the regenerator while the magnetic field is high, absorbing heat from the material and rejecting it to the hot reservoir. This is followed by the adiabatic demagnetization, which further decreases the temperature of the material, allowing it to reach temperatures below that of the surrounding ambient. Lastly, fluid from the hot reservoir enters the regenerator, losing heat to the MCM, lowering its temperature and allowing it to absorb heat from the cold reservoir, finishing the cycle. This operation results in a complex system involving heat transfer, fluid mechanics, materials sciences and magnetism in which several aspects of the design of the AMR and the synchronization between each step of the cycle needs to be taken into account in order

to obtain the best performance possible (Vieira *et al.*, 2023).

An important factor that also affects the performance is the temperature profile along the regenerator since, as mentioned above, the MCE is maximized near the Curie temperature of the material and thus, ideally, the material would only operate near this temperature. The relevance of this profile may be higher or lower depending on the type of material: first-order materials, like La-Fe-Si alloys, have a very large magnetocaloric effect near the Curie temperature, but almost none when not close enough to it, while second-order materials, like Gd, do not have a magnetocaloric effect as large as their counterpart, but present a considerable MCE even at temperatures relatively far from their Curie temperature (Smith *et al.*, 2012; Bez, 2016). Because of this, it is common practice to divide first-order AMRs into several layers with different Curie temperatures that try to follow the expected temperature profile during operation. However, because the layers are normally designed with the final temperature span in mind, the layering of the material may hinder the pull-down process in which the whole regenerator starts at a constant temperature and most of it can be expected to underperform before the final temperature span is reached. If this underperformance is severe enough, the system may never reach the desired temperature span.

A possible solution for this problem is the use of hybrid regenerators, i.e., regenerators comprised of both Gd and La-Fe-Si alloys. Ideally, in this configuration, the Gd layer(s) would allow the system to reach the desired span during pull-down due to the characteristics of second-order materials while also allowing the AMR to reach the higher cooling capacities usually associated with first-order materials. The first step to achieve this would be to develop an accurate model of hybrid regenerators which could then be used to determine some of the important design parameters of the AMR for its given operating conditions, including the amount of Gd that should be added to it. In this work, an attempt to take this first step was made by adapting the numerical model developed by Trevizoli (2015) and further modified by Lang (2018) and Vieira (2020) to be able to simulate hybrid regenerators. This new model was then used to simulate a hybrid regenerator that was tested in a well-established AMR testing apparatus and the results were compared in order to validate the model.

A total of three frequencies, two blow fractions and four different mass flow rates were tested, with the numerical and experimental results showing good agreement in most cases. The highest frequency cases had the worst agreement of all, with the difference being attributed to limitations of the experimental apparatus to operate under these conditions. Some experimental results showed an inconsistent behaviour attributed to possible corrosion of the material due to extended idle periods. The model was, however, able to generally predict the shape of the cooling capacity curves and maximum temperature span reached by the regenerator. The absolute agreement was generally better for higher mass flow rates and never exceeded 8.2 W in terms of cooling capacity.

2. Numerical Model

The numerical model employed is an improved version of the numerical model developed by Trevizoli (2015) and further modified by Lang (2018) and Vieira (2020). It utilizes an unidimensional porous medium approach to solve the fluid momentum equation and the coupled energy equations for each phase. For the momentum equation, the flow is assumed to be laminar and incompressible, flowing in a low porosity medium and with negligible body forces, resulting in the simplified equation:

$$\frac{\rho_\mathrm{f}}{\varepsilon_\mathrm{eff}}\left(\frac{\partial u}{\partial t}\right) = -\frac{\partial P}{\partial x} - \frac{\mu_\mathrm{f}}{K}u - \frac{c_\mathrm{E}\rho_\mathrm{f}}{K^{1/2}}|u|u \tag{1}$$

where the terms represent, from left to right, the macroscopic inertia of the flow, the pressure gradient, the microscopic viscous shear stress and the microscopic inertial force. ρ_f is the fluid density, u is the Darcy velocity, t is the time, P is the pressure, x is the axial position, μ_f is the fluid viscosity, K is the permeability of the porous medium and c_E is the Ergun constant. In this equation, instead of the regular definition of porosity, an effective porosity, ε_eff, is used, which is adjusted through experimental pressure drop data to better predict the hydraulic behaviour of the regenerator.

The fluid phase energy equation is given by:

$$\rho_\mathrm{f} c_\mathrm{f}\left(\varepsilon\frac{\partial T_\mathrm{f}}{\partial t} + u\frac{\partial T_\mathrm{f}}{\partial x}\right) = h\beta(T_\mathrm{s} - T_\mathrm{f}) + \left|u_\mathrm{D}\frac{\partial P}{\partial x}\right| + \varepsilon[k_\mathrm{f} + \rho_\mathrm{f} c_\mathrm{f} D_{||}]\frac{\partial^2 T_\mathrm{f}}{\partial x^2}, \tag{2}$$

where the terms represent, from left to right, the thermal capacity, the longitudinal advection, the interstitial heat transfer, the viscous dissipation and the axial diffusion and porous medium dispersion. c_f is the fluid specific heat capacity, T_f is the fluid temperature, h is the interstitial heat transfer coefficient, β is the interstitial heat transfer area density, T_s is the solid temperature, k_f is the fluid thermal conductivity and $D_{||}$ is the longitudinal thermal dispersion. Note that, in this case, the regular porosity, ε, is used.

Finally, the solid phase energy equation is given by:

$$\rho_\mathrm{s} c_\mathrm{s}(1-\varepsilon)\frac{\partial T_\mathrm{s}}{\partial t} = h\beta(T_\mathrm{f} - T_\mathrm{s}) + (1-\varepsilon)k_\mathrm{s}\frac{\partial^2 T_\mathrm{s}}{\partial x^2} + \dot{q}_\mathrm{MCE}, \tag{3}$$

where the terms represent, from left to right, the thermal capacity, the interstitial heat transfer, the axial diffusion and the magnetocaloric effect. c_{s} is the solid specific heat capacity and k_{s} is the solid thermal conductivity. Note that, in this case, the magnetocaloric effect is represented by a heat generation term through the so-called *built-in* approach (Trevizoli *et al.*, 2016), being given by:

$$\dot{q}_{\mathrm{EMC}} = -\rho_{\mathrm{s}} T_{\mathrm{s}} (1-\varepsilon) \frac{\partial s_{\mathrm{s}}}{\partial B} \frac{\partial B}{\partial t} \tag{4}$$

where s_{s} is the solid specific entropy and B is the magnetic flux density.

The fluid phase properties were assumed to be those of deionized water given that, as will be discussed in the following section, the mixture was mostly comprised of water. The solid phase properties were interpolated from the data obtained by Vieira *et al.* (2021). Several Nusselt number correlations were tested to determine interstitial heat transfer coefficient, including the ones developed by Gunn (1978), Wakao and Kaguei (1982), and Kuwahara *et al.* (2001), but the one that had the best agreement with previous experimental tests was the one developed by Pallares and Grau (2010), which was used in all simulations presented in this work. Other closure relationships used in the model, including the one for the demagnetization factor, can be found in Trevizoli *et al.* (2016), Vieira (2020) and Vieira *et al.* (2021).

The model used in this work solves the conservation equations presented above through the finite volume method, using the regenerator geometry and mass flow rate as inputs and returning, among other things, the pressure drop and temperature profiles, which can then be used to determine performance parameters of interest, like the cooling capacity. The main improvement made to the model in this work when compared to the original one mentioned in the beginning of this section is that, while generating the unidimensional mesh, the improved model is capable of associating a different value of porosity, interstitial heat transfer coefficient, demagnetization factor, type of material and magnetocaloric properties to each volume, allowing it to simulate an AMR with layers comprised of completely different materials, instead of only the same material with different Curie temperatures.

3. Experimental Apparatus

3.1 Regenerator

The AMR employed in the validation consisted of a 24.2 mm diameter stainless steel case filled with ten layers of magnetocaloric material with different Curie temperatures ranging from 290.00 K to 314.55 K. The first layer on the cold side of the regenerator and largest layer overall was comprised of pure Gd, while the other nine layers were comprised of La-Fe-Si alloys supplied by Vacuumschmelze with Curie temperatures ranging from 290.65 K next to the Gd layer to 314.55 K on the other end of the regenerator, arranged in ascending order. The length, mass and Curie temperature of each layer in order from the cold side to the hot side can be found in Table 1.

Table 1. Composition, Curie temperature, layer length and mass of all layers in the test regenerator.

Composition	**Curie temperature**	**Length**	**Mass**
Gd	290.00 K	28.57 mm	65.33 g
$\mathrm{La(Fe,Mn,Si)_{13}H_z}$	290.65 K	7.14 mm	11.50 g
$\mathrm{La(Fe,Mn,Si)_{13}H_z}$	294.05 K	7.14 mm	12.21 g
$\mathrm{La(Fe,Mn,Si)_{13}H_z}$	297.55 K	7.14 mm	12.21 g
$\mathrm{La(Fe,Mn,Si)_{13}H_z}$	300.55 K	7.14 mm	11.50 g
$\mathrm{La(Fe,Mn,Si)_{13}H_z}$	303.15 K	7.14 mm	12.21 g
$\mathrm{La(Fe,Mn,Si)_{13}H_z}$	306.65 K	7.14 mm	12.91 g
$\mathrm{La(Fe,Mn,Si)_{13}H_z}$	309.65 K	7.15 mm	11.97 g
$\mathrm{La(Fe,Mn,Si)_{13}H_z}$	310.95 K	7.15 mm	11.99 g
$\mathrm{La(Fe,Mn,Si)_{13}H_z}$	312.45 K	7.15 mm	12.22 g
$\mathrm{La(Fe,Mn,Si)_{13}H_z}$	314.55 K	7.15 mm	12.17 g

3.2 AMR testing

A schematic representation of the AMR experimental apparatus is presented in Fig 1. This apparatus was first developed by Trevizoli *et al.* (2016), and later improved by Nakashima *et al.* (2017), Hoffmann (2020) and Teza *et al.* (2021). The apparatus may be divided into four sub-systems: (i) a magnetic circuit comprised of two concentric Halbach cylinders which yield a maximum magnetic flux density of 1.69 T in the gap where the AMR is placed, (ii) two thermal baths capable of emulating ideal heat exchangers, (iii) a gear pump and two pairs of solenoid valves responsible for generating and directing the flow, and (iv) a control system capable of setting the mass flow rate, the AMR operation frequency and the blow fractions (i.e., the percentage of the total cycle period in which a blow is actually happening). Within the control

system, there are two Coriolis mass flow meters responsible for measuring the mass flow rate of each blow, pressure transducers responsible for measuring the pressure drop within the AMR and thermocouples at both ends of the regenerator responsible for measuring the inlet and outlet temperature profiles. This experimental data can then be used to determine important performance parameters such as the cooling capacity, the rejected heat and the pumping power. The fluid used in all tests was a mixture consisting of 95% vol. of water and 5% vol. of a commercial anti-corrosive substance called ME-1.

The testing procedure consisted of initially specifying a cold side temperature (290 K, matching the Curie temperature of the Gd layer) and then setting the other relevant operating parameters: mass flow rate, frequency and blow fraction. Initially, the temperature span was 0 K and thus the hot side temperature is equal to the cold side's. The regenerator was then submitted to the AMR cycle until cyclic equilibrium was reached, after which the experimental data started being recorded for 20 cycles. The results were then processed in order to determine, among other parameters, the average cooling capacity of the 20 cycles. The hot side temperature (and, consequently, the temperature span) was then increased by 4 K and the same procedure was done in order to determine the new cooling capacity. This procedure was repeated until the cooling capacity reached zero.

In this work, a total of 16 different operating conditions were tested from span 0 K until the cooling capacity was depleted: 4 tests had a frequency of 0.5 Hz and a blow fraction of 50 % with the mass flow rate ranging from 20 kg/h to 80 kg/h in steps of 20 kg/h, 4 tests had a frequency of 0.75 Hz and a blow fraction of 50 % with the same mass flow rates mentioned before, and 4 tests had a frequency of 0.5 Hz and a blow fraction of 37.5 % with yet again the same mass flow rates mentioned.

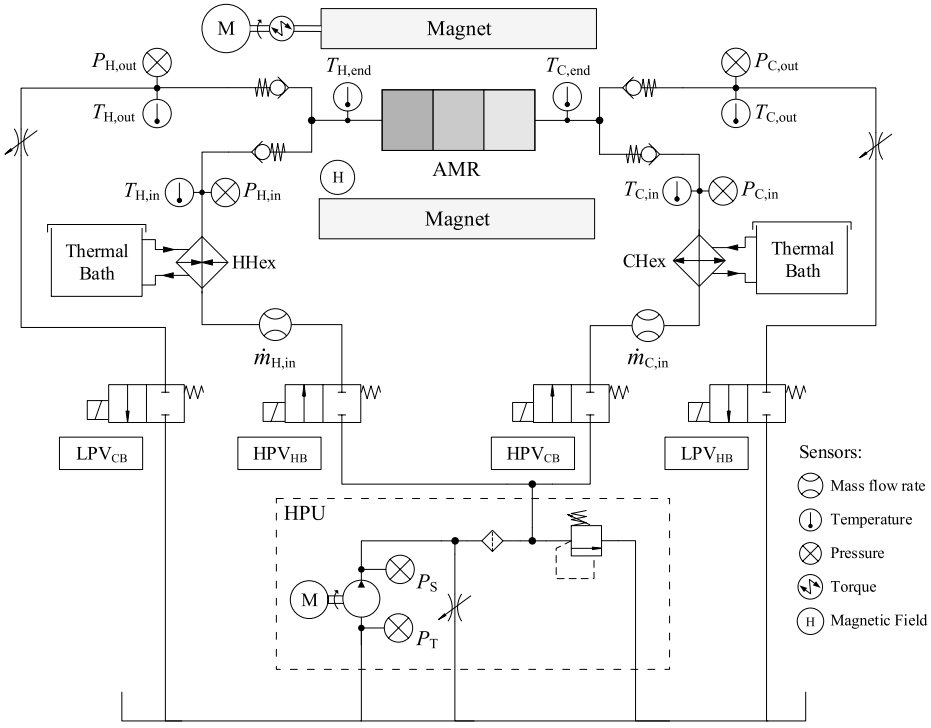

Figure 1. Schematic representation of the apparatus employed in the experimental characterization (Vieira *et al.*, 2021)

4. Results

In order to validate the model described in Section 2, all experimental test conditions were also run in the model in order to compare the cooling capacities given by each approach. The final results are shown in Figures 2 to 5. It can be seen that, regardless of the other operating conditions, in cases with low mass flow rate, especially 20 kg/h, the model has a clear tendency to overestimate the experimental results. This discrepancy was also observed in other tests of non-hybrid regenerators and so is believed to be an inherent behaviour of the model itself and not specifically of the hybrid approach.

Regarding the tests at 0.5 Hz with a blow fraction of 50%, the model showed considerable accuracy for average to high mass flow rates, accurately predicting the maximum temperature span reached in all cases and the general shape of the cooling capacity curve for the cases at 40 kg/h and 60 kg/h. The maximum deviation was approximately 6.0 W for 20 kg/h, 7.0 W for 40 kg/h, 3.0 W for 60 kg/h and 8.0 W for 80 kg/h.

The tests at 0.25 Hz with a blow fraction of 50%, while overall worse regarding the performance of the regenerator, had an even better agreement between the model and the experiments. In all cases the model was able to follow the

performance curve and, when this point was reached, predict the maximum temperature span reached by the regenerator. The maximum deviation was approximately 4.6 W for 20 kg/h, 5.3 W for 40 kg/h, 2.6 W for 60 kg/h and 5.6 W for 80 kg/h.

The tests at he tests at 0.75 Hz with a blow fraction of 50% had the worst agreement of all, with only the results at 80 kg/h showing a relatively good correspondence. Nevertheless, the model was still able to predict the shape of the curve and the maximum temperature span. The reason for the worse correspondence in this case may not be related to the model, but to the apparatus itself, which had previously shown irregularities in measurement at higher frequencies, like 0.75 Hz.

Finally, the tests at 0.25 Hz and blow fraction of 37.5% showed a good agreement once again, with the model capturing the shape of the curve, maximum temperature span and cooling capacity values. The maximum deviation was approximately 4.2 W for 20 kg/h, 8.2 W for 40 kg/h, 3.8 W for 60 kg/h and 5.4 W for 80 kg/h. The large deviation for the 40 kg/h scenario is a byproduct of a phenomenon only observed in these tests, where some experimental points presented a large deviation from their expected curve. This is believed to have been caused by corrosion of the material, which had to stay idle for approximately 2 months due to complications with the apparatus. For reference, Table 2 shows the beginning and end dates of all experiments, with all other tests taking less than a week to be completed. If these deviations are indeed caused by corrosion of the material, making these outlier results not-representative of the regenerator, the maximum deviation for the 40 kg/h test was of 4.5 W.

It is also important to highlight the temperature spans that the regenerator was able to reach both experimentally and numerically. In general, first-order regenerators are expected to reach temperature spans roughly equal to the difference between their largest and smallest Curie temperatures, which would be around 24.5 K in this case. The results, however, were regularly capable of reaching temperature spans over 30 K at different operating conditions. This is an indication that the addition of a Gd layer does in fact help the regenerator to operate even under less than optimal temperature conditions, which is the main goal of this configuration. More tests, however, are needed to confirm that this configuration also improves the pull-down performance of magnetic refrigeration systems.

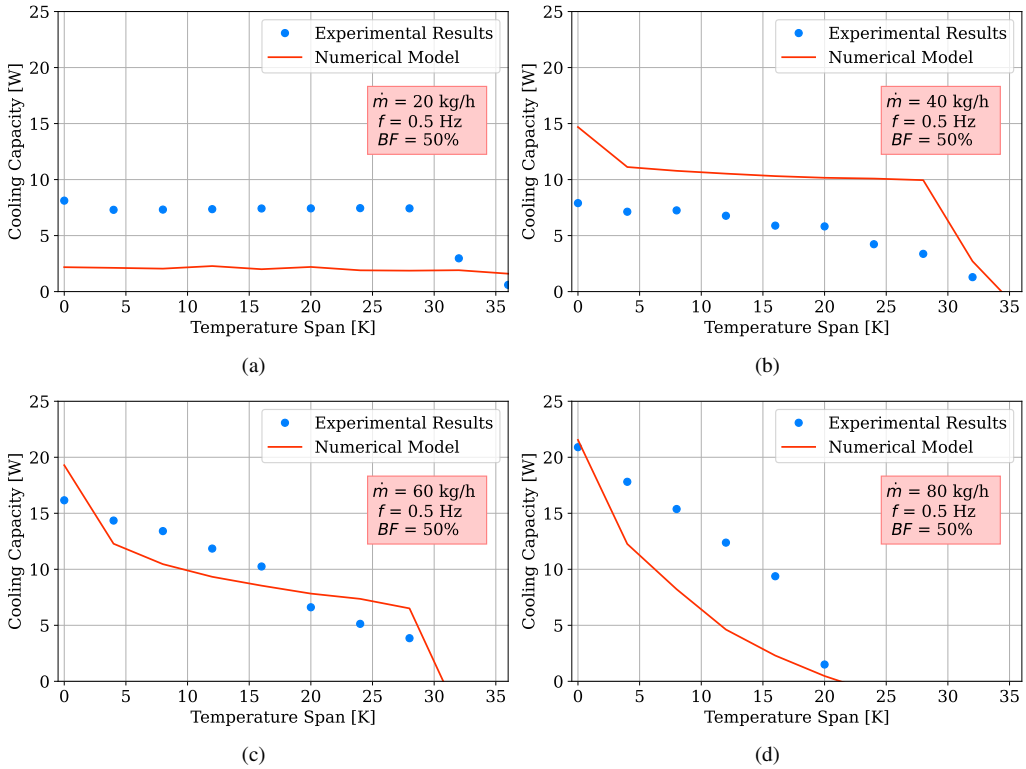

Figure 2. Numerical and experimental results for and AMR frequency of 0.5 Hz with a blow fraction of 50% and a mass flow rate of (a) 20 kg/h, (b) 40 kg/h (c) 60 kg/h and (d) 80 kg/h.

5. Conclusion

In this work, an AMR numerical model was adapted to allow for the simulation of hybrid regenerators, i.e., regenerators comprised of more than one kind of magnetocaloric material. This was achieved by allowing each control volume on the mesh to have its own physical and geometrical properties. This model was then used to simulate an existing hybrid regenerator comprised of one large layer of Gd and 10 layer of La-Fe-Si alloys which was then experimentally tested in

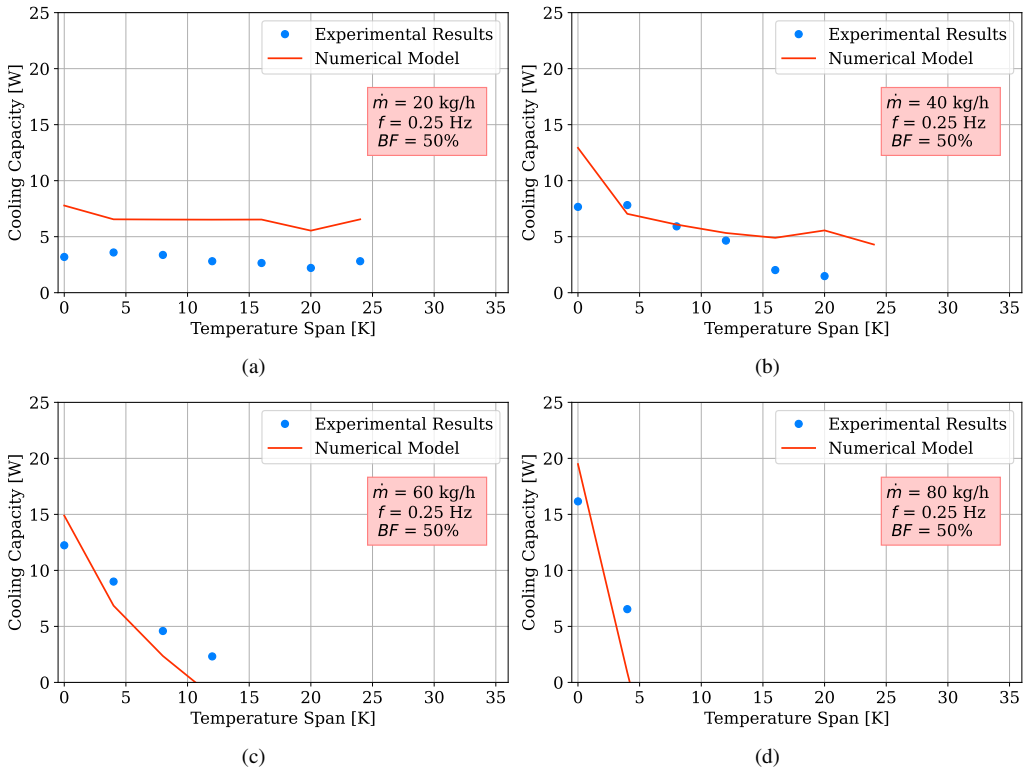

Figure 3. Numerical and experimental results for an AMR frequency of 0.25 Hz with a blow fraction of 50% and mass flow rate of (a) 20 kg/h, (b) 40 kg/h (c) 60 kg/h and (d) 80 kg/h.

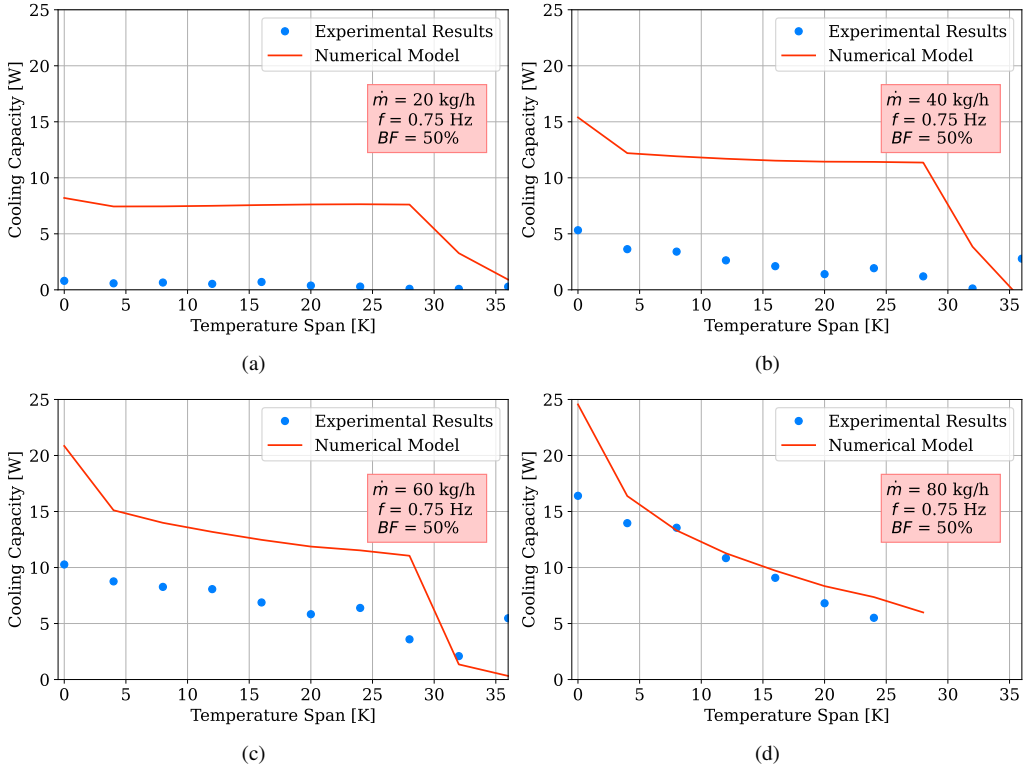

Figure 4. Numerical and experimental results for an AMR frequency of 0.75 Hz with a blow fraction of 50% and mass flow rate of (a) 20 kg/h, (b) 40 kg/h (c) 60 kg/h and (d) 80 kg/h.

a pre-existing AMR testing apparatus. The results were then compared, presented and discussed. The model was very accurate regarding the behaviour, i.e., shape of the cooling capacity curve and the maximum temperature span, but was not always able to accurately predict the precise value of the cooling capacity, especially for low mass flow rates. High

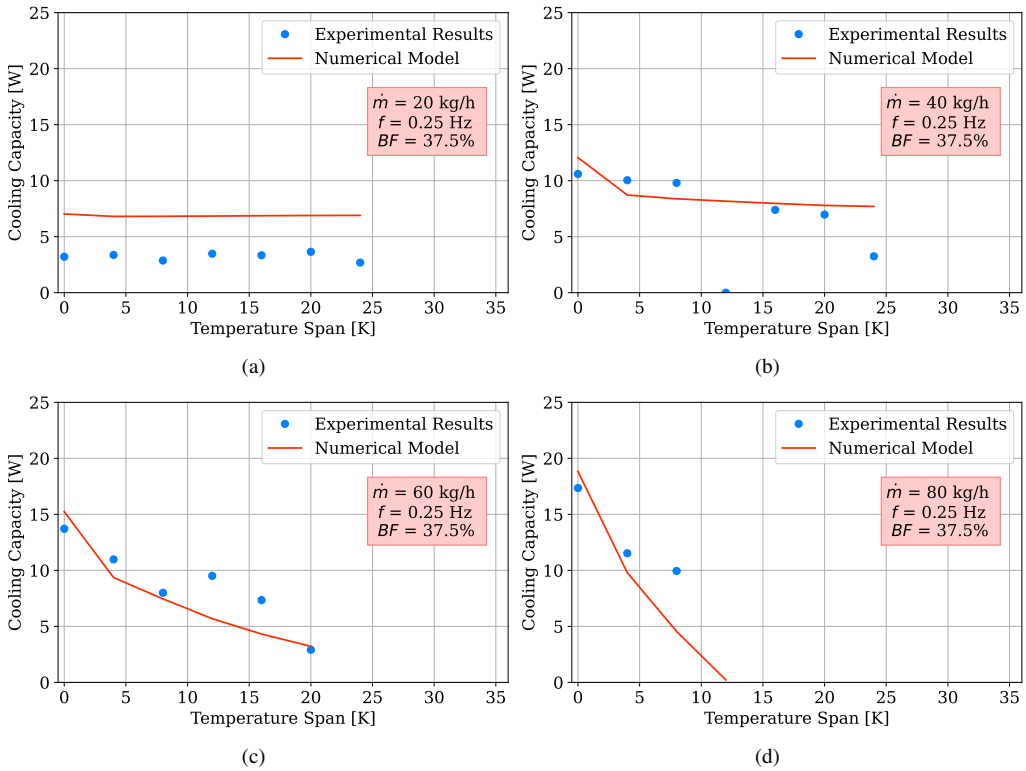

Figure 5. Numerical and experimental results for an AMR frequency of 0.25 Hz with a blow fraction of 37.5% and mass flow rate of (a) 20 kg/h, (b) 40 kg/h (c) 60 kg/h and (d) 80 kg/h.

Table 2. Beginning and final dates of the experimental tests.

Corresponding figure	Frequency	BF	MFR	Start date	Final date
2 (a)	0.50	50%	20 kg/h	14 oct 2022	20 oct 2022
2 (b)	0.50	50%	40 kg/h	14 oct 2022	20 oct 2022
2 (c)	0.50	50%	60 kg/h	14 oct 2022	20 oct 2022
2 (d)	0.50	50%	80 kg/h	14 oct 2022	18 oct 2022
3 (a)	0.25	50%	20 kg/h	20 oct 2022	24 oct 2022
3 (b)	0.25	50%	40 kg/h	20 oct 2022	24 oct 2022
3 (c)	0.25	50%	60 kg/h	20 oct 2022	24 oct 2022
3 (d)	0.25	50%	80 kg/h	20 oct 2022	21 oct 2022
4 (a)	0.75	50%	20 kg/h	25 oct 2022	04 nov 2022
4 (b)	0.75	50%	40 kg/h	25 oct 2022	04 nov 2022
4 (c)	0.75	50%	60 kg/h	25 oct 2022	04 nov 2022
4 (d)	0.75	50%	80 kg/h	25 oct 2022	27 oct 2022
5 (a)	0.25	37.5%	20 kg/h	11 nov 2022	09 jan 2023
5 (b)	0.25	37.5%	40 kg/h	11 nov 2022	09 jan 2023
5 (c)	0.25	37.5%	60 kg/h	11 nov 2022	09 jan 2023
5 (d)	0.25	37.5%	80 kg/h	08 dec 2022	16 dec 2022

frequency cases also had a worse agreement than others, a behaviour that was attributed to limitations of the apparatus when operating under these conditions. Some results were also hindered by possible corrosion associated with long idle times due to complications with the testing apparatus. Despite these challenges, however, the agreement between model and experiment was considered promising, never surpassing 8.2 W with maximum cooling capacities reaching values of up to 25 W. The experiments also showed that the hybrid regenerator was able to reach higher temperature spans than the ones expected from their regular first-order counterpart, a promising result for the application of this technology in new magnetic refrigeration applications.

Acknowledgements

The authors acknowledge the financial support from m CNPq, FAPESC, CAPES, CODEMGE and the EMBRAPII Unit Polo/UFSC.

REFERENCES

Bez, H.N., 2016. *Magnetocaloric materials and first order phase transitions*. Ph.D. thesis, Technical University of Denmark.

Bjørk, R., Bahl, C.R.H. and Katter, M., 2010. "Magnetocaloric properties of $LaFe_{13-x-y}Co_xSi_y$ and commercial grade gd". *Journal of Magnetism and Magnetic Materials*, Vol. 322, pp. 3882–3888. doi:10.1016/j.jmmm.2010.08.013.

Gunn, D., 1978. "Transfer of heat or mass to particles in fixed and fluidised beds". *International Journal of Heat and Mass Transfer*, Vol. 21, pp. 467–476. ISSN 00179310. doi:10.1016/0017-9310(78)90080-7.

Hansen, B.R., Kuhn, L.T., Bahl, C.R.H., Lundberg, M., Ancona-Torres, C. and Katter, M., 2010. "Properties of magnetocaloric la(fe,co,si)13 produced by powder metallurgy". *Journal of Magnetism and Magnetic Materials*, Vol. 322, pp. 3447–3454. doi:10.1016/j.jmmm.2010.06.043.

Hoffmann, G., 2020. "Estudo e desenvolvimento de estratégias de controle para sistemas de refrigeração magnética".

Kitanovski, A., Tusek, J., Tomc, U., Plaznik, U., Ozbolt, M. and Poredos, A., 2015. *Magnetocaloric Energy Conversion from Theory to Applications*. Springer.

Kuwahara, F., Shirota, M. and Nakayama, A., 2001. "A numerical study of interfacial convective heat transfer coefficient in two-energy equation model for convection in porous media". *International Journal of Heat and Mass Transfer*, Vol. 44, pp. 1153–1159. ISSN 00179310. doi:10.1016/S0017-9310(00)00166-6.

Lang, G.B., 2018. "Development of an active magnetic regenerator model using the finite volumes method for a magnetic refrigeration application."

Nakashima, A., Hoffmann, G., Lozano, J., Barbosa, J. and Dutra, S.L., 2017. "Using electrovalves as a flow distribution system for an active magnetic regenerator". *Procceedings of the 24th ABCM International Congress of Mechanicl Engineering*.

Pallares, J. and Grau, F., 2010. "A modification of a nusselt number correlation for forced convection in porous media". *International Communications in Heat and Mass Transfer*, Vol. 37, pp. 1187–1190. ISSN 07351933. doi: 10.1016/j.icheatmasstransfer.2010.07.014.

Smith, A., Bahl, C.R., Bjørk, R., Engelbrecht, K., Nielsen, K.K. and Pryds, N., 2012. "Materials challenges for high performance magnetocaloric refrigeration devices". *Advanced Energy Materials*, Vol. 2, pp. 1288–1318.

Teza, H.F., Vieira, B.P., de Sá, N.M., Nakashima, A.T.D., Peixer, G.F., , Lozano, G.H.J.A. and Jr., J.R.B., 2021. "Characterization of the thermo-hydraulic performance of a $La(Fe,Mn,Si)_{13}H_y$ regenerator". *Procceedings of the 26th ABCM International Congress of Mechanicl Engineering*.

Trevizoli, P., 2015. *Development of Thermal Regenerators for Magnetic Cooling Applications*. Ph.D. thesis.

Trevizoli, P.V., Nakashima, A.T. and Barbosa, J.R., 2016. "Performance evaluation of an active magnetic regenerator for cooling applications – part ii: Mathematical modeling and thermal losses". *International Journal of Refrigeration*, Vol. 72, pp. 206–217. ISSN 01407007. doi:10.1016/j.ijrefrig.2016.07.010.

Vieira, B.P., 2020. *Modeling and optimization of active magnetic regenerators using La-Fe-Si based alloys*. Ph.D. thesis.

Vieira, B.P., Bez, H.N., dos Santos, D., Lozano, J.A. and Jr, J.R.B., 2023. "Interrelationship between flow profiles and the magnetic waveform and their influence on the performance of first-order active magnetic regenerators". *Applied Thermal Engineering*, Vol. 219.

Vieira, B.P., Bez, H.N., Kuepferling, M., Rosa, M.A., Schafer, D., Cid, C.C.P., Vieyra, H.A., Basso, V., Lozano, J.A. and Jr, J.R.B., 2021. "Magnetocaloric properties of spheroidal $La(Fe,Mn,Si)_{13}H$ granules and their performance in epoxy-bonded active magnetic regenerators". *Applied Thermal Engineering*, Vol. 183.

Wakao, N. and Kaguei, S., 1982. *Heat and mass transfer in packed beds.* Gordon and Breach Science.

6. RESPONSIBILITY NOTICE

The authors are solely responsible for the printed material included in this paper.